Electronic Supplementary Information

Expansion of multifunctionality in off-stoichiometric manganite using post-annealing and high pressure: physical and electrochemical studies

Zhiwei Gong[a], Wei Xu[b], N. A. Liedienov[*,a,c], D. S. Butenko[d], I. V. Zatovsky[*,e,f], I. A. Gural'skiy[g], Ziyu Wei[h], Quanjun Li[a], Bingbing Liu[a], Yu. A. Batman[i], A. V. Pashchenko[a,c,j], G. G. Levchenko[*,a,c]

[a]*State Key Laboratory of Superhard Materials, International Center of Future Science, Jilin University, 130012 Changchun, China*
[b]*State Key Laboratory of Inorganic Synthesis and Preparative Chemistry, College of Chemistry, Jilin University, 130012 Changchun, China*
[c]*Donetsk Institute for Physics and Engineering named after O.O. Galkin, NASU, 03028 Kyiv, Ukraine*
[d]*Academy for Advanced Interdisciplinary Studies, Southern University of Science and Technology, 518055 Shenzhen, China*
[e]*College of Physics, Jilin University, 130012 Changchun, China*
[f]*F.D. Ovcharenko Institute of Biocolloidal Chemistry, NASU, 03142 Kyiv, Ukraine*
[g]*Taras Shevchenko National University of Kyiv, 01601 Kyiv, Ukraine*
[h]*College of Physics Science and Technology, Heilongjiang University, 150080 Harbin, China*
[i]*Bogomolets National Medical University, 01601 Kyiv, Ukraine*
[j]*Institute of Magnetism NASU and MESU, 03142 Kyiv, Ukraine*

* Corresponding author
E-mail address: nikita.ledenev.ssp@gmail.com (N.A. Liedienov)
zvigo@ukr.net (I.V. Zatovsky)
g-levch@ukr.net (G.G. Levchenko)

ESI1

XRD, elemental composition, and XPS of the LMO ceramics

Table S1

Atomic positions for the LMO samples annealed at different temperatures t_{ann}.

t_{ann}	**LMO-1150**		**LMO-1250**	**LMO-1350**		**LMO-1450**
	LMO(*R*-3*c*)	Mn_3O_4	LMO(*R*-3*c*)	LMO(*Pnma*)	LMO(*R*-3*c*)	LMO(*Pnma*)
	La1(6a)	Mn1(4a)	La1(6a)	La1(4c)	La1(6a)	La1(4c)
	occ. 0.9		occ. 0.9	occ. 0.9	occ. 0.9	occ. 0.9
x	0	0	0	0.0368(4)	0	0.0368(4)
y	1	0.25	1	0.25	1	0.25
z	0.25	-0.125	0.25	0.9958(9)	0.25	0.9958(9)
	Mn1(6b)	Mn2(8d)	Mn1(6b)	Mn1(4b)	Mn1(6b)	Mn1(4b)
x	0.333	0	0.333	0	0.333	0
y	0.6667	0.5	0.6667	0	0.6667	0
z	0.1667	0.5	0.1667	0.5	0.1667	0.5
	Mn2(6a)	O1(16h)	Mn2(6a)	Mn2(4c)	Mn2(6a)	Mn2(4c)
	occ. 0.1		occ. 0.1	occ. 0.1	occ. 0.1	occ. 0.1
x	0	0	0	0.0368(4)	0	0.0368(4)
y	1	0.47	1	0.25	1	0.25
z	0.25	0.259	0.25	0.9958(9)	0.25	0.9958(9)
	O1(18e)		O1(18e)	O1(4c)	O1(18e)	O1(4c)
x	0.471(15)		0.471(15)	0.003(4)	0.471(15)	0.003(4)
y	1		1	-0.25	1	-0.25
z	0.25		0.25	0.599(4)	0.25	0.599(4)
				O2(8d)		O2(8d)
x				0.2915(25)		0.2915(25)
y				0.0340(21)		0.0340(21)
z				0.734(4)		0.734(4)

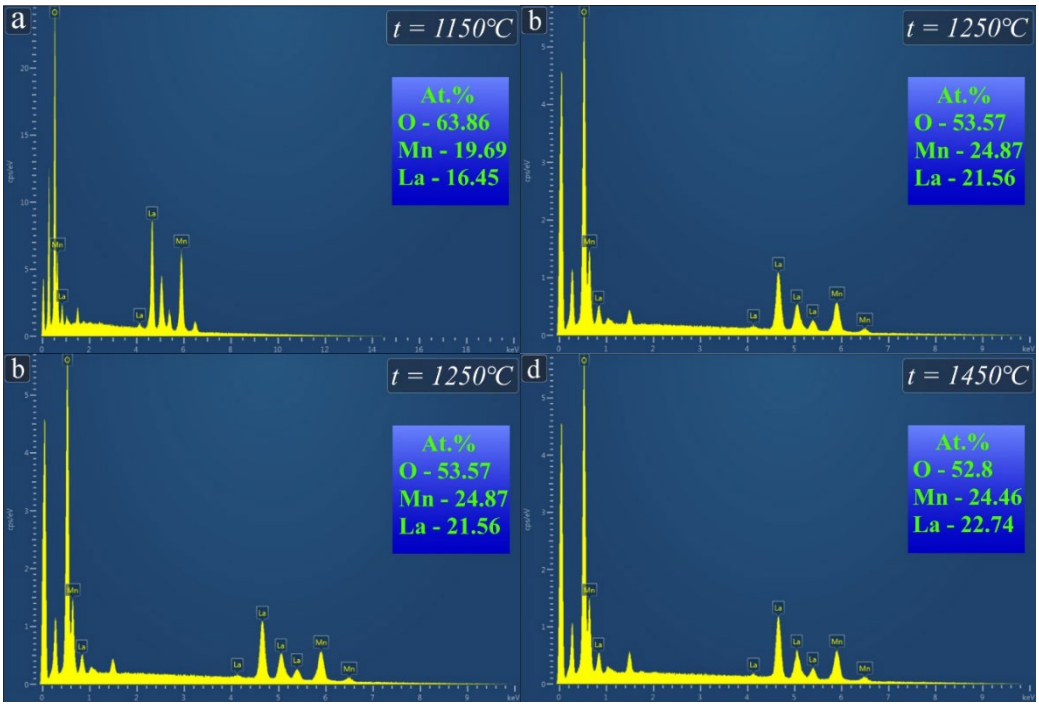

Fig. S1. EDS data for the LMO-1150 (a), LMO-1250 (b), LMO-1350 (c), and LMO-1450 (d).

The survey spectra of LMO samples show the existence of La, Mn, and O peaks (Fig. S2(a, b)). In the high-resolution XPS spectra of La3d, two major peaks are observed, which belong to the spin doublet $La3d_{5/2}$ and $La3d_{3/2}$ (Fig. S2(c)). However, the spectra have a more complex profile due to the presence of charge transfer satellites (Fig. S2(c)), plasmon lines, and MNN Auger lines (marked as A and B in Fig. S2(c)). Similar results are also observed for the XPS spectrum of La_2O_3 [1] and La-containing manganite compounds [2]. The binding energy spectrum for LMO-1150 and LMO-1450 samples are in the range of 833.8-833.9 eV ($La3d_{5/2}$) and 850.7-850.9 eV ($La3d_{3/2}$), respectively. The positions for all peaks are listed in Table S2. As for O1s XPS (Fig. S2(d)), three components with energy positions about 529.5 (A), 530.9 (B), and 532.8 (C) eV can be distinguished in the spectrum (see Table S2). Peak A should be attributed to the oxygen of the magnetite crystal lattice, while components B and C are due to adsorbed oxygen and hydroxyl groups or water on the surface, respectively [2].

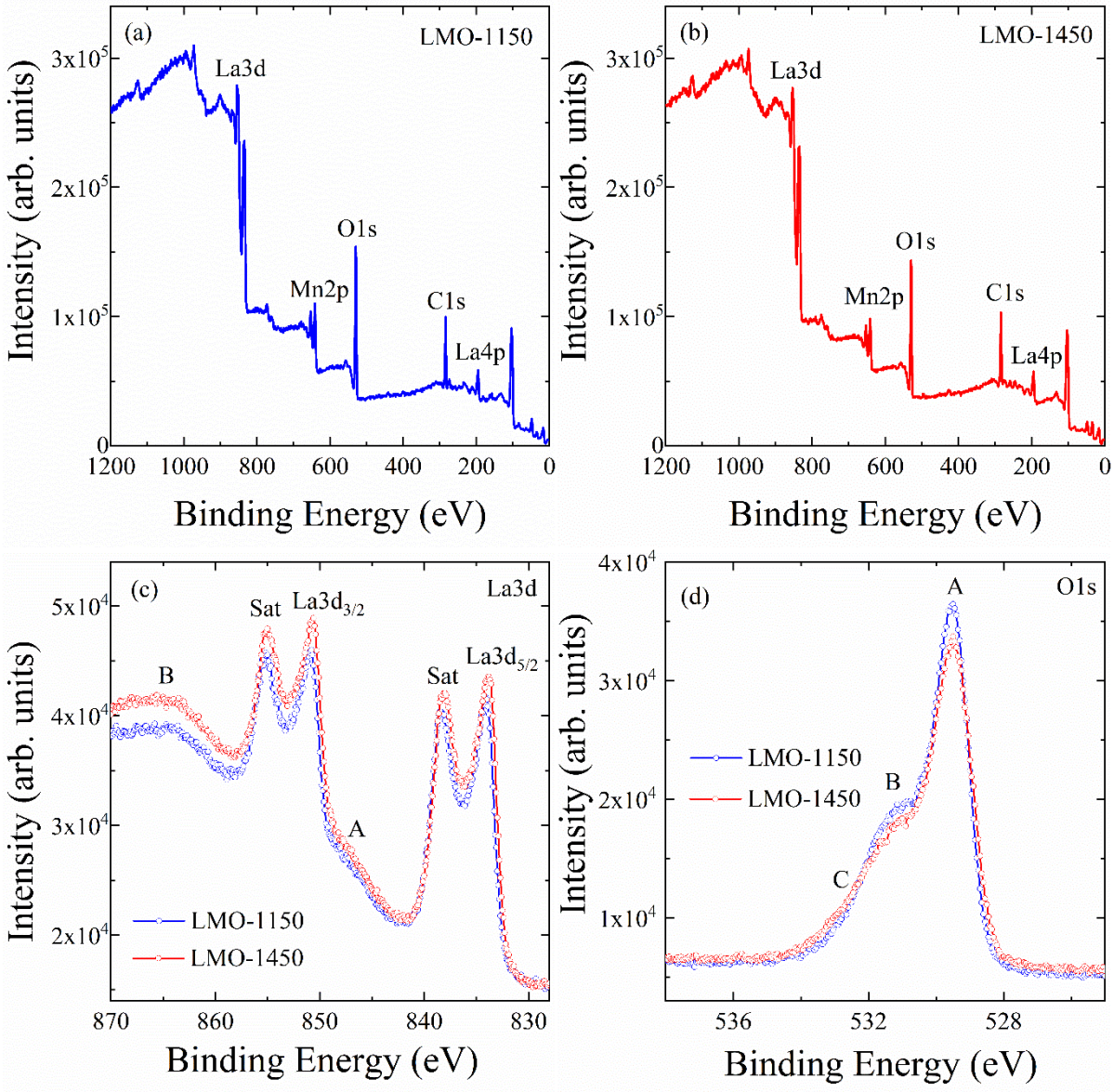

Fig. S2. XPS curves for the LMO-1150 and LMO-1450 compounds: (a) and (b) survey spectrum; (c) La3d spectrum; and (d) O1s spectrum.

Table S2

Energy positions of the La3d, O1s and Mn2p$_{3/2}$ X-ray photoelectron lines in the LMO samples.

t_{ann} (°C)	Binding energy (eV)												
	La3d				O1s			Mn2p$_{3/2}$			Mn2p$_{1/2}$		
	La3d$_{5/2}$	Sat	La3d$_{3/2}$	Sat	A	B	C	Mn^{2+}	Mn^{3+}	Mn^{4+}	Mn^{2+}	Mn^{3+}	Mn^{4+}
1150	833.9	838.3	850.9	855.2	529.5	530.9	532.8	641.3	641.9	642.8	651.9	653.5	655.3
1450	833.8	838.0	850.7	855.0	529.4	530.9	532.5	641.0	641.7	642.7	651.9	653.5	655.3

ESI2

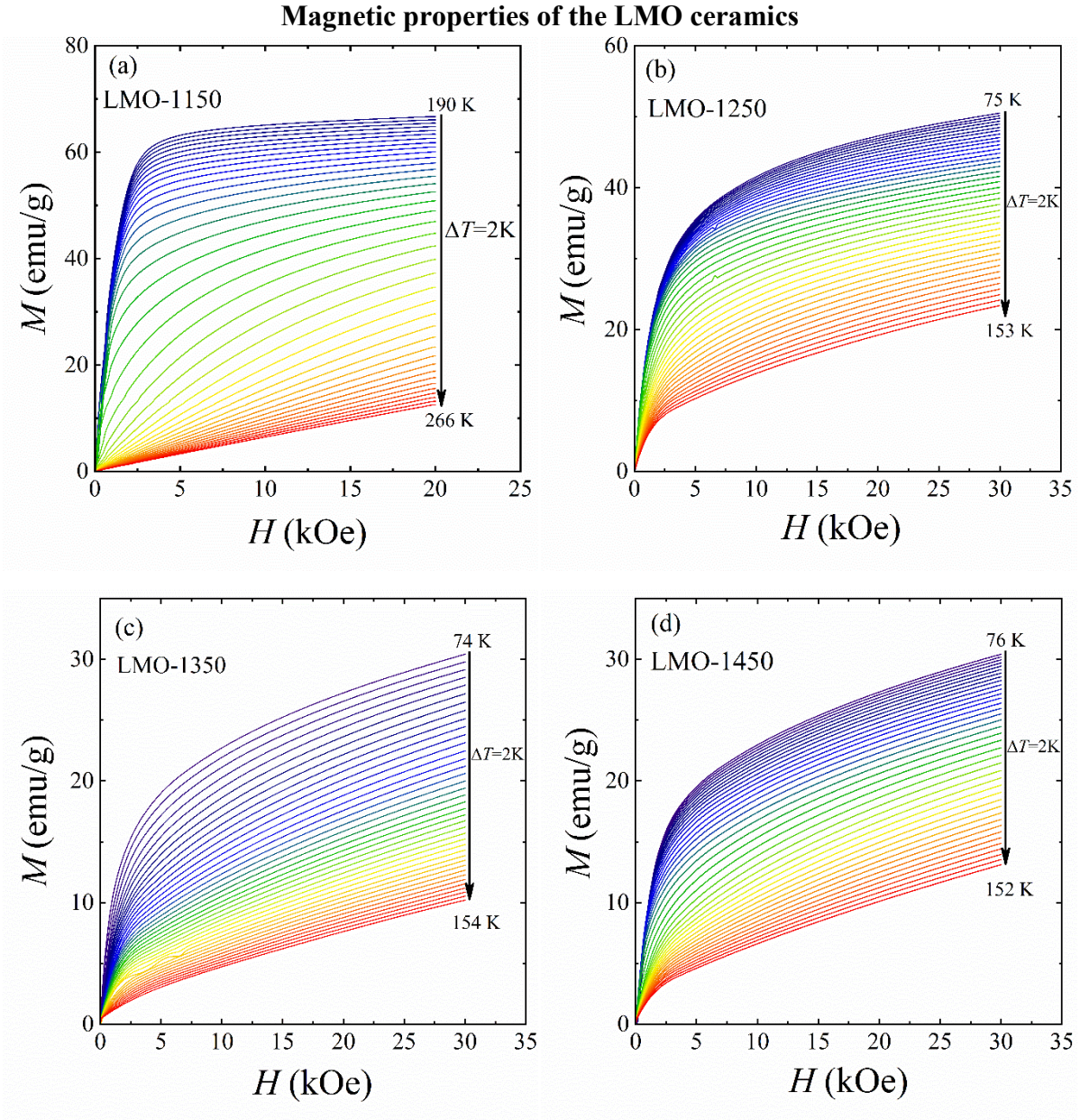

Fig. S3. Isotherms of magnetization $M(H)$ for the LMO-1150 (a), LMO-1250 (b), LMO-1350 (c), and LMO-1450 (d).

Magnetic properties of the LMO-1150 ceramics under high pressure

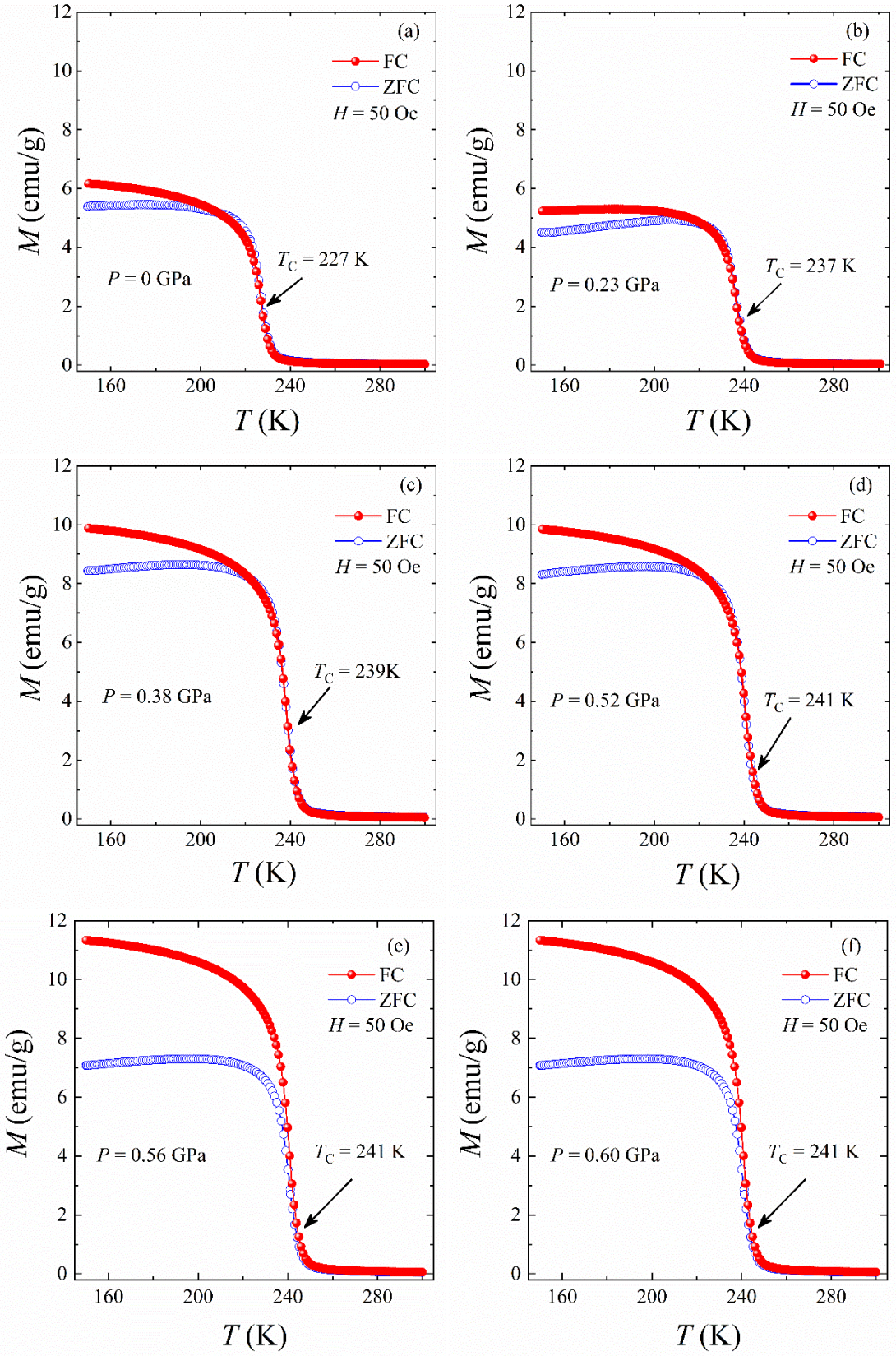

Fig S4. Temperature dependences of $M_{FC}(T)$ and $M_{ZFC}(T)$ at the field of H = 50 Oe for the LMO-1150 under different pressures P = 0 GPa (a), 0.23 GPa (b), 0.38 GPa (c), 0.52 GPa (d), 0.56 GPa (e), and 0.60 GPa (f).

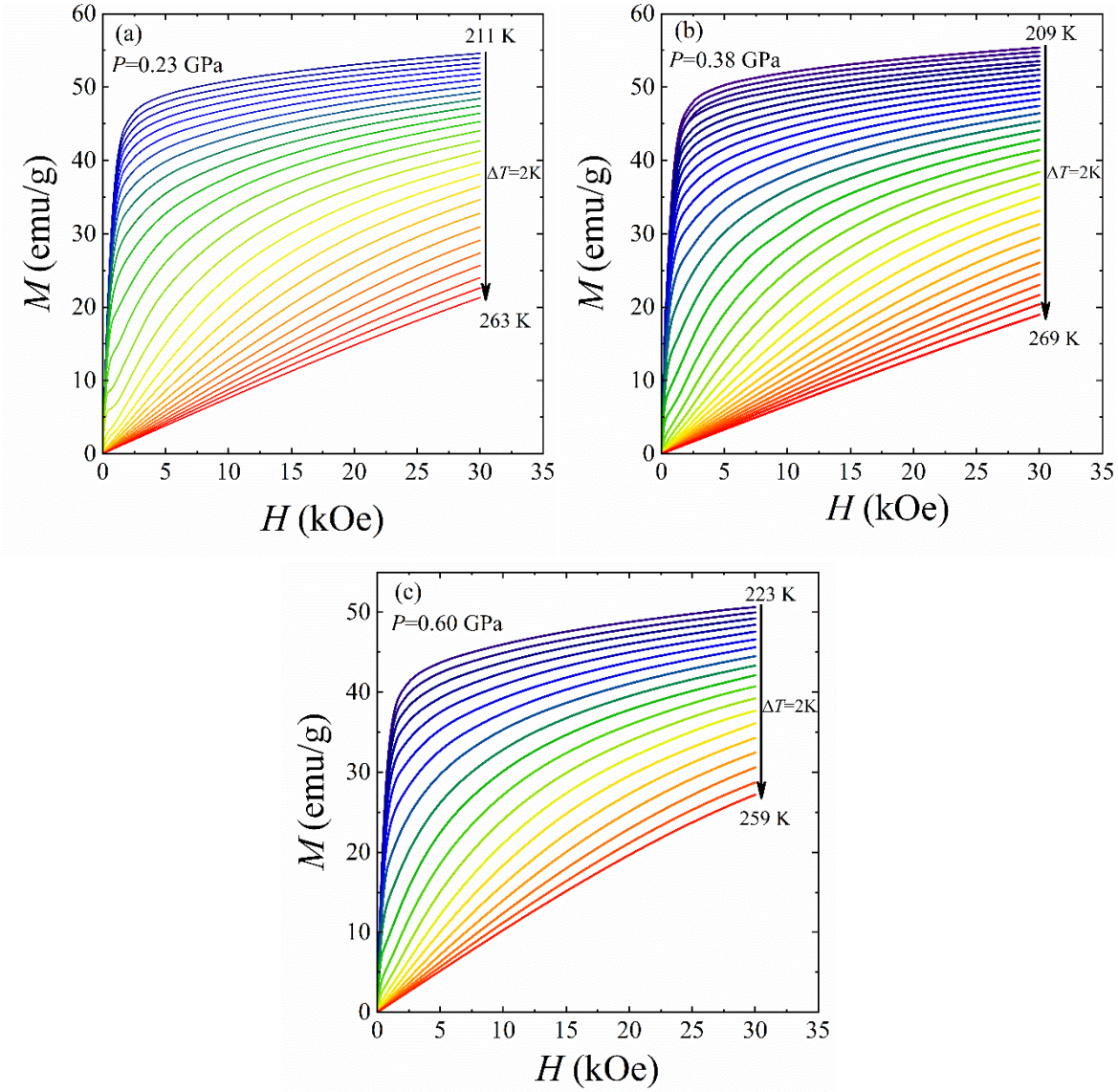

Fig S5. Isotherms of the magnetization $M(H)$ for the LMO-1150 under different pressures P = 0.23 GPa (a), 0.38 GPa (b), and 0.60 GPa (c).

ESI4

Electrochemical properties of the LMO ceramics

Calibrated with respect to RHE Ag/AgCl electrode was used as the reference electrode. The calibration was performed in a high purity hydrogen saturated electrolyte with a Pt foil as the working electrode. CV curves were run at a scan rate of 1 $mV \cdot s^{-1}$, and the average of the two potentials, when current crossed zero was taken to be the thermodynamic potential for the hydrogen electrode reactions. The potential measured against the Ag/AgCl electrode was converted according to the Nernst equation:

$$E_{vs.\ RHE} = E_{vs.\ Ag/AgCl} + 0.197 + 0.052pH.$$

The RHE potential was for different electrolytes calculated as

$$E_{vs.\ RHE} = E_{vs.\ Ag/AgCl} + 0.6114V \text{ (for 0.5 M } K_2SO_4 \text{ solution, pH = 7.0);}$$

$$E_{vs.\ RHE} = E_{vs.\ Ag/AgCl} + 0.6884V \text{ (for 0.5 M } K_2HPO_4 \text{ solution, pH = 8.3);}$$

$$E_{vs.\ RHE} = E_{vs.\ Ag/AgCl} + 0.7416V \text{ (for 0.1 M } K_2B_4O_7 \text{ solution, pH = 9.2).}$$

The overpotential (η) is calculated as the following equation: $\eta = E_{vs.\ RHE} - 1.23$ V.

All tests were performed in a climate controlled electrochemical laboratory (temperature within 20–22 °C, atmospheric humidity 30–40%).

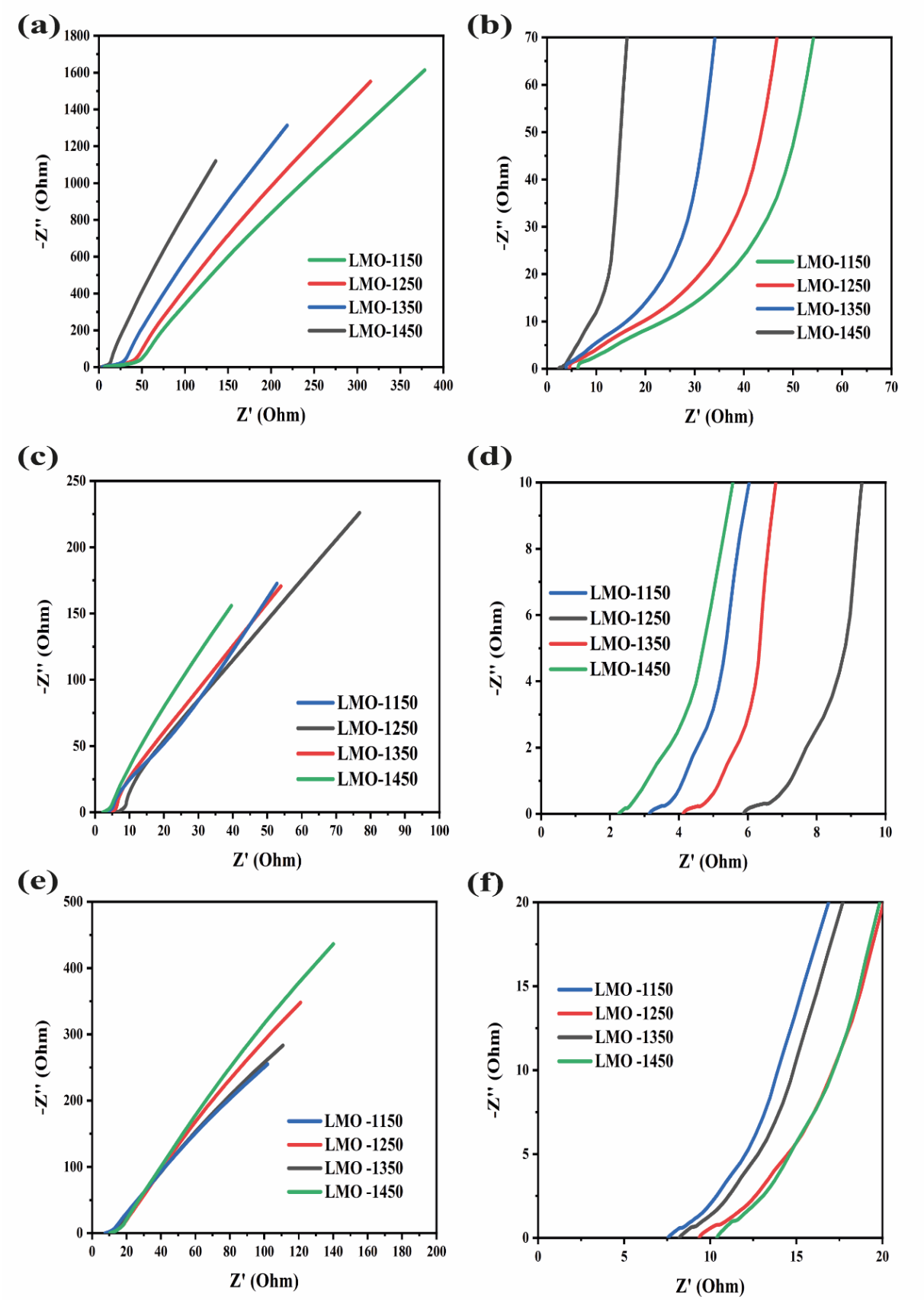

Fig. S6. Electrochemical impedance spectroscopy (AC) of the LMO materials in different electrolytes: 0.5 M K_2SO_4 (a, b), 0.5 M K_2HPO_4 (c, d), and 0.1 M $K_2B_4O_7$ (e, f).

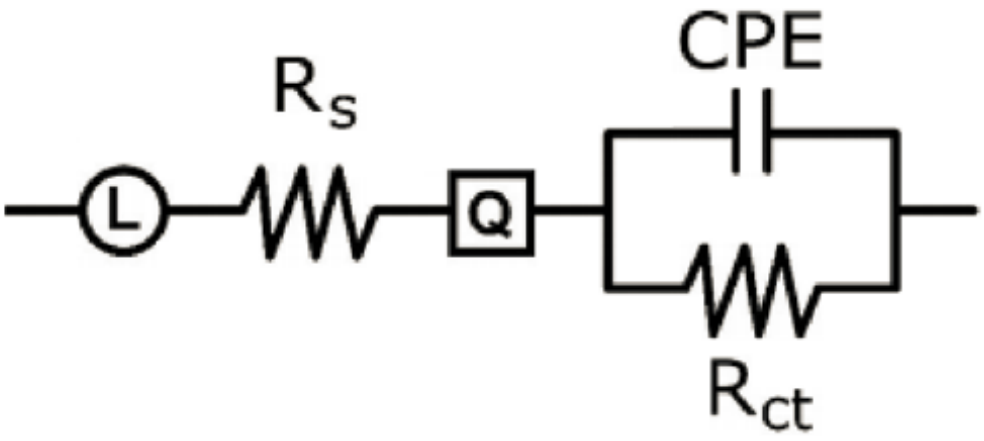

Fig. S7. The equivalent scheme for EIS measurement.

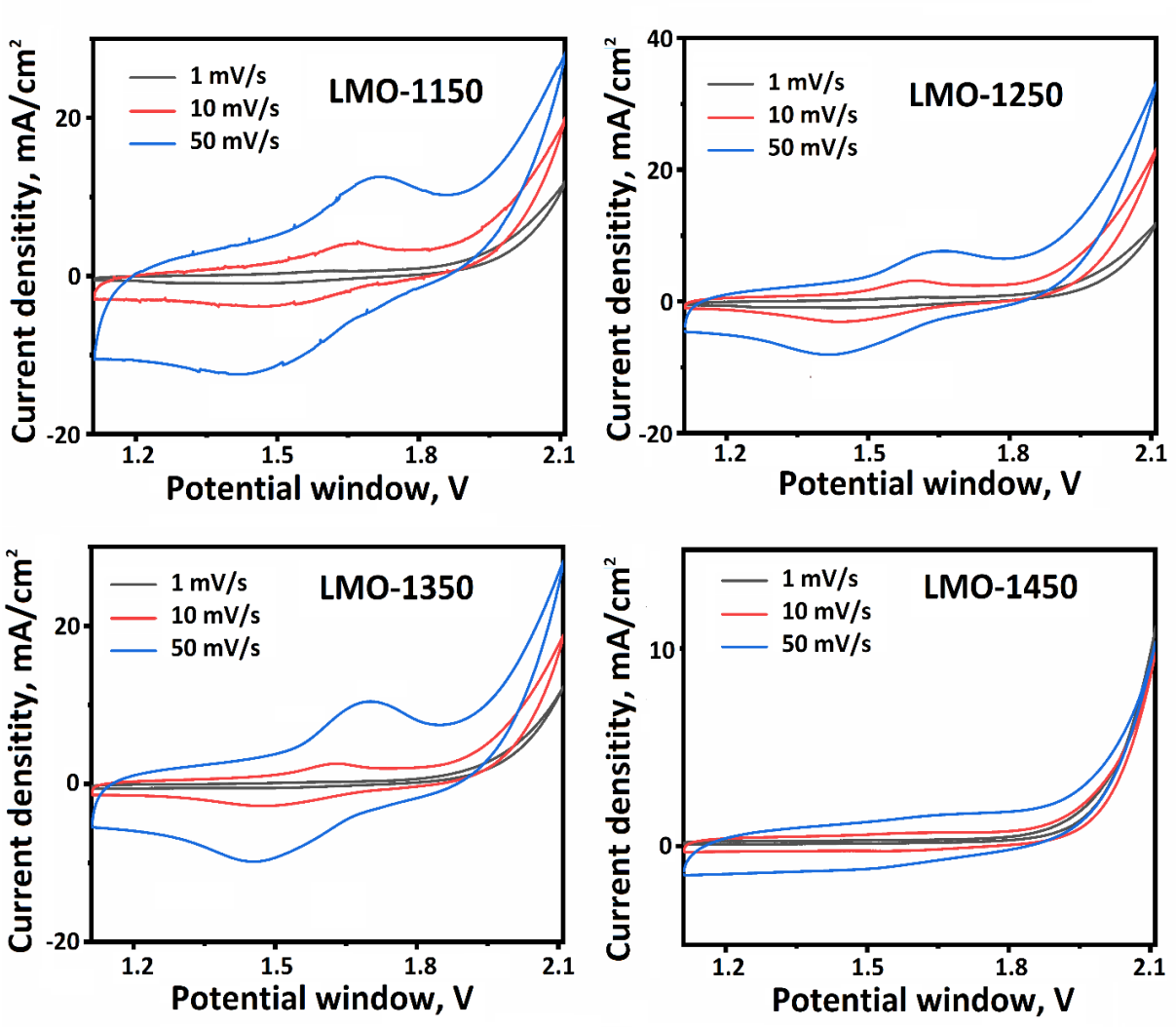

Fig. S8. CV curves for the LMO samples at different scan rates in 0.5 M K_2SO_4 electrolyte (potential window from 0.74 to 2.25 V *vs* RHE).

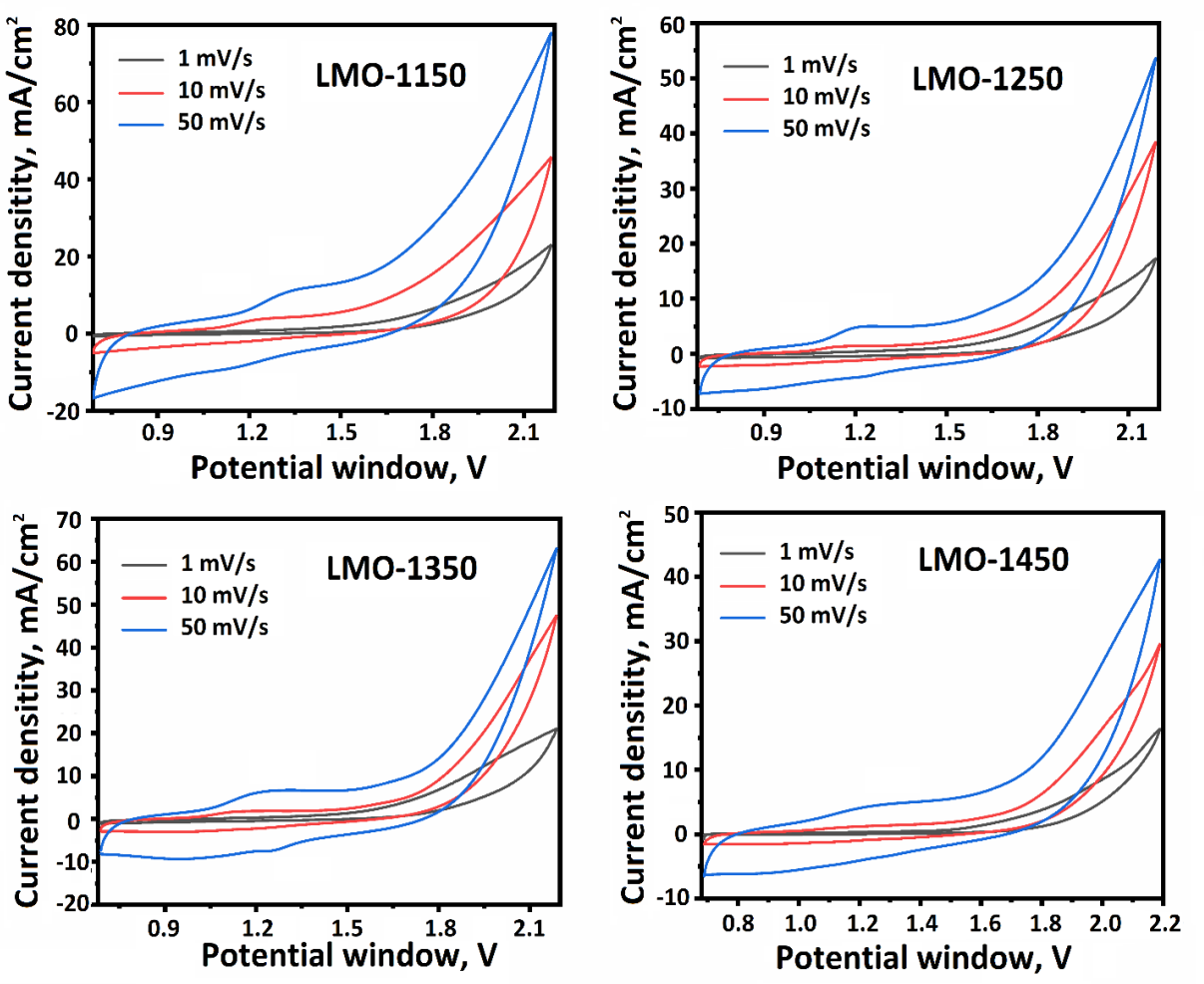

Fig. S9. CV curves for the LMO samples at different scan rates in 0.5 M K_2HPO_4 electrolyte (potential window from 0.69 to 2.20 V *vs* RHE).

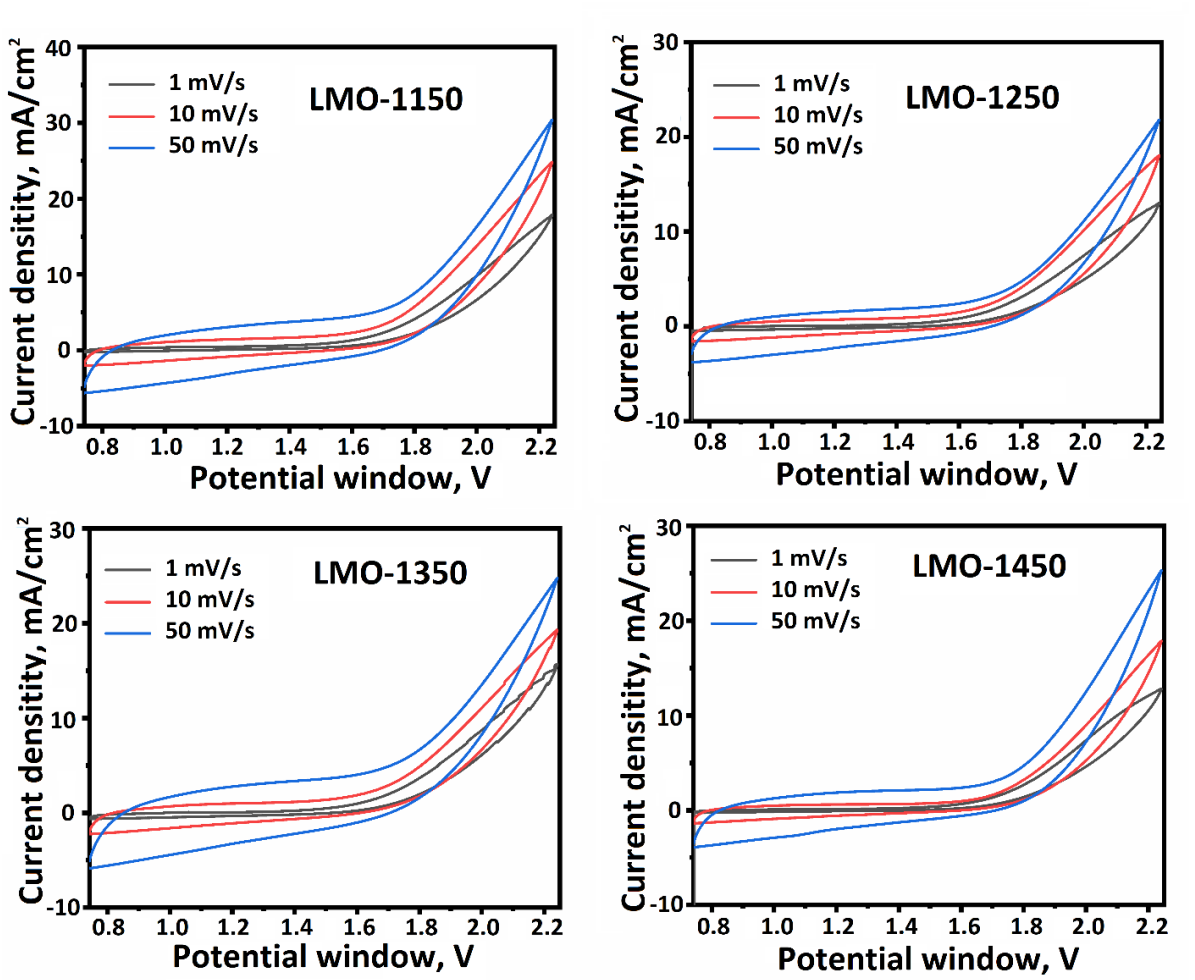

Fig. S10. CV curves for the LMO samples at different scan rates in 0.1 M $K_2B_2O_7$ electrolyte (potential window from 0.74 to 2.25 V *vs* RHE).

Table S3

OER activity for LMO at current density of 5 and 10 mA/cm^2 in different electrolytes.

Electrolyte	Overpotential (mV) Current density of 5/10 (mA/cm^2)			
	LMO-1150	LMO-1250	LMO-1350	LMO-1450
K_2SO_4 (0.5 M)	734/827	693/770	734/813	767/827
K_2HPO_4 (0.5 M)	445/615	465/674	453/641	600/674
$K_2B_4O_7$ (0.1 M)	577/786	606/836	562/747	642/836

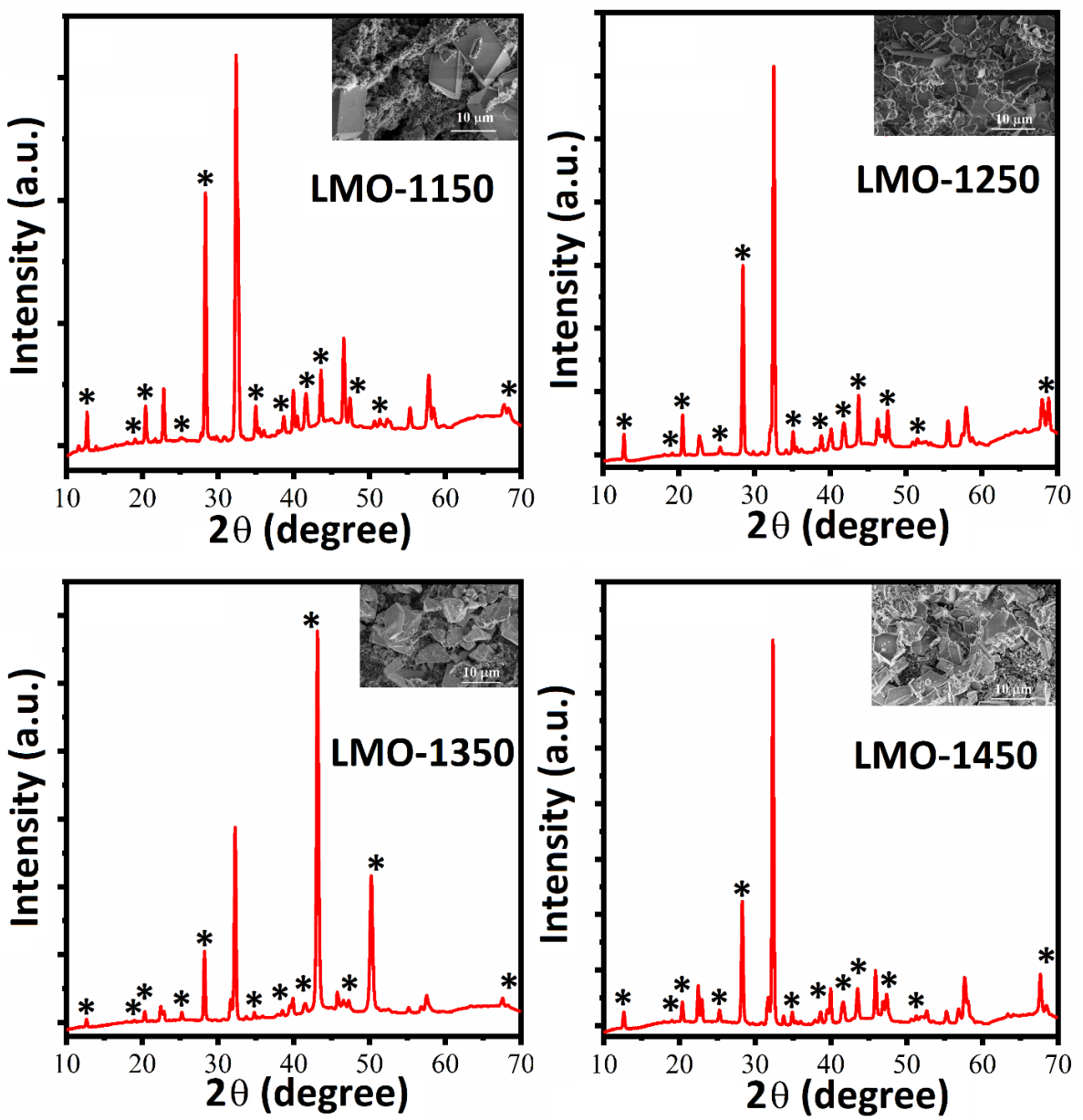

Fig. S11. The XRD results for the LMO electrode after CP test in 0.5 M K_2SO_4 electrolyte (* denotes $K_{10}La_2(SO_4)_8$, PDF-2 #00-033-1019). The insets are the SEM images.

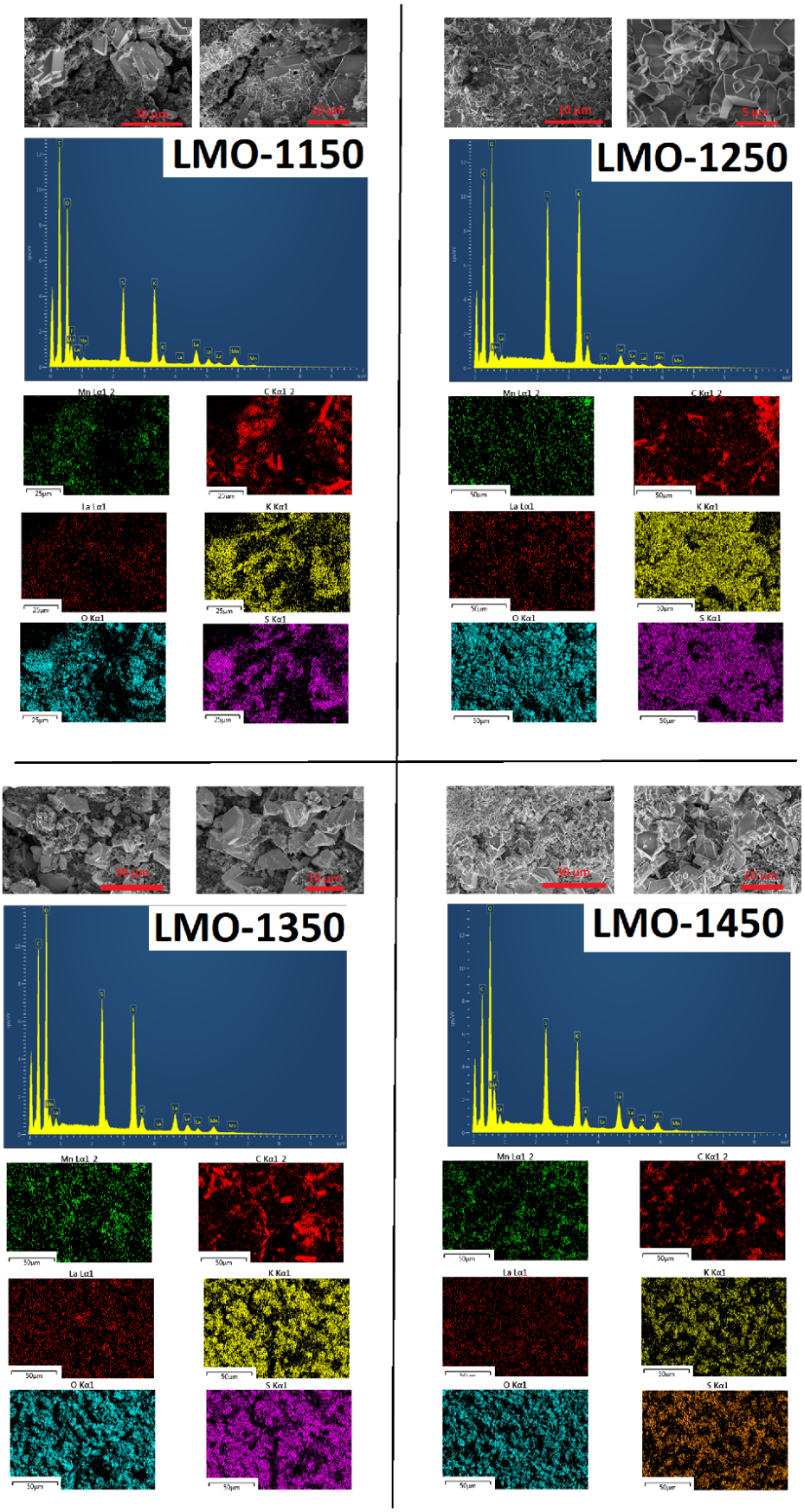

Fig. S12. SEM images, EDS and elemental mapping for the LMO electrodes after CP test in 0.5 M K_2SO_4 electrolyte.

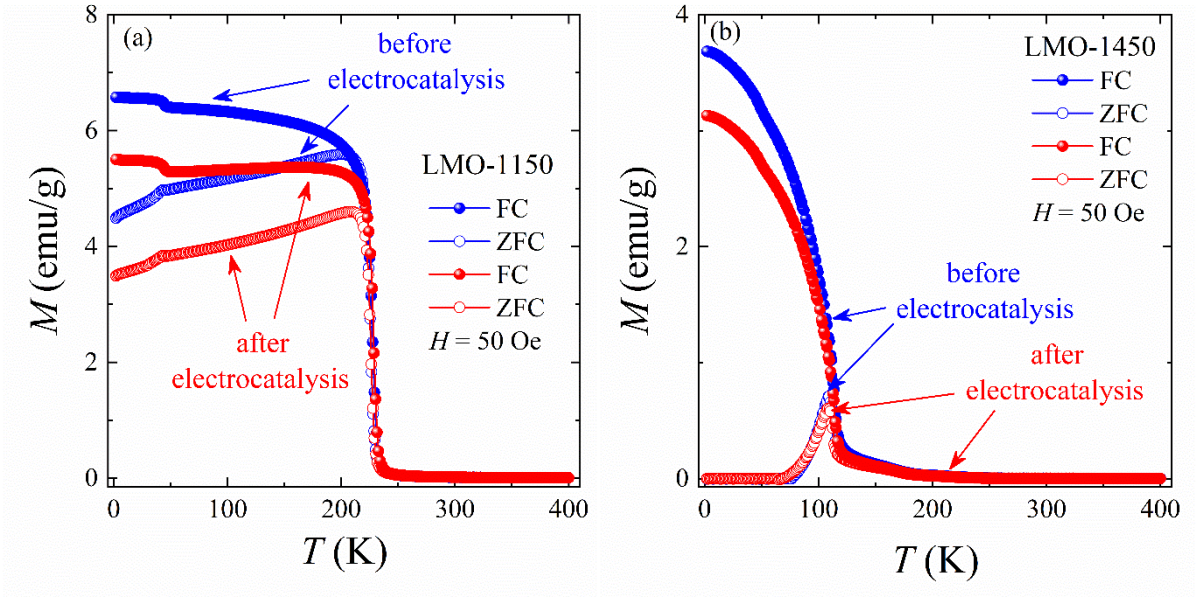

Fig. S13. Temperature dependences of $M_{FC}(T)$ and $M_{ZFC}(T)$ in the field of H = 50 Oe for the LMO-1150 (a) and LMO-1450 (b) before and after electrocatalysis in K_2SO_4 (0.5 M) media at 10 mA/cm^2 for 8 h.

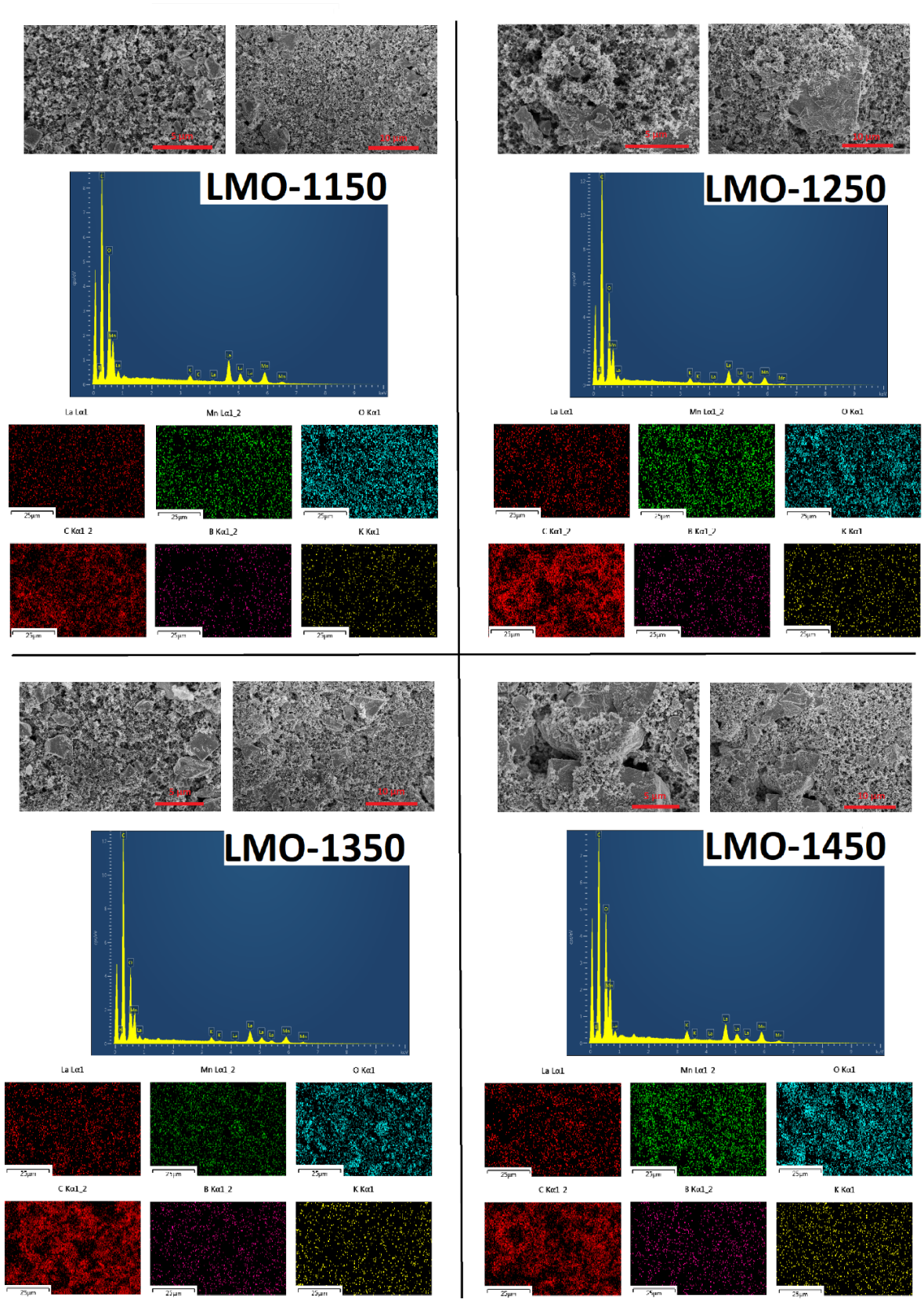

Fig. S14. SEM images, EDS and elemental mapping for the LMO electrodes after CP test in 0.1 M $K_2B_2O_7$ electrolyte.

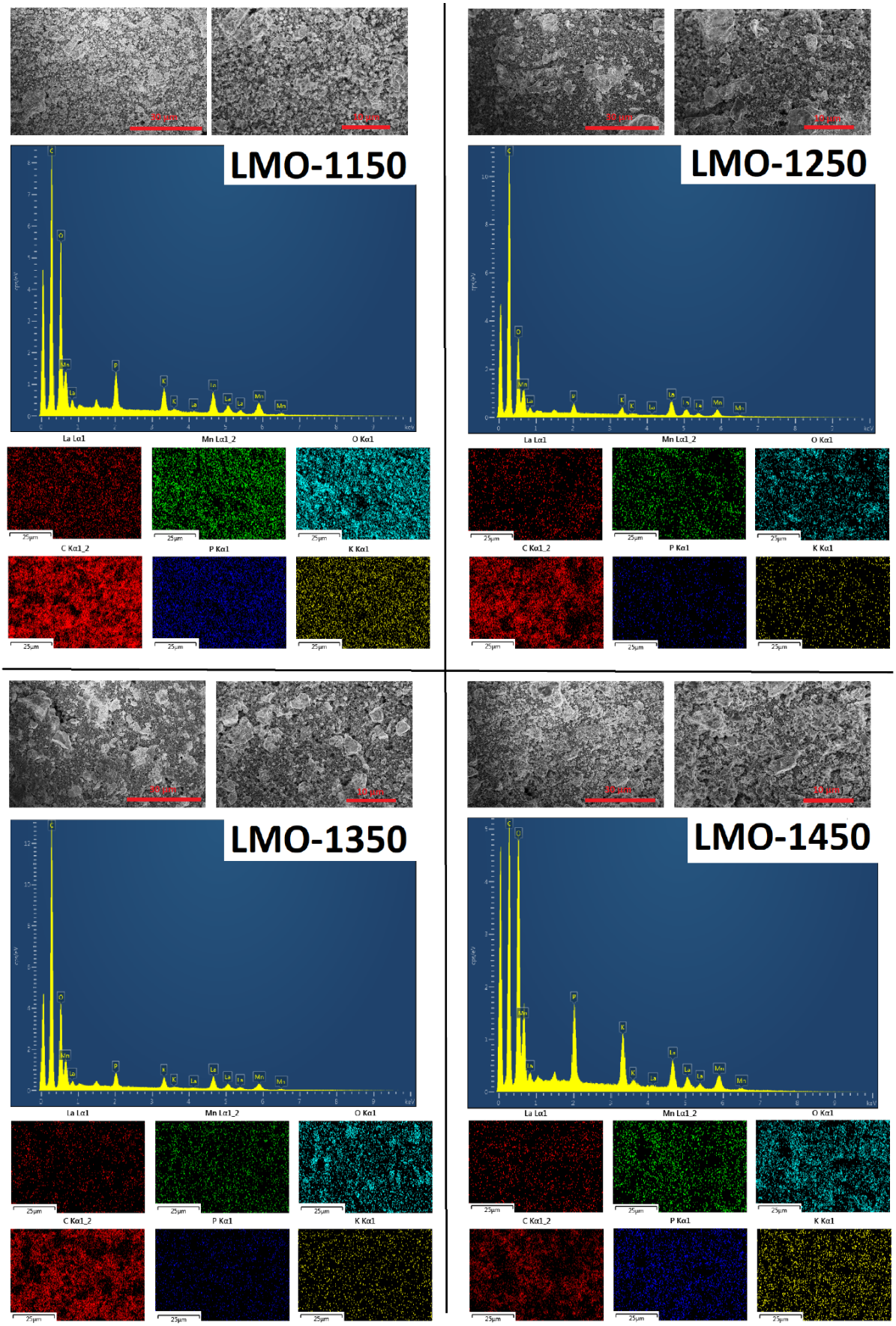

Fig. S15. SEM images, EDS and elemental mapping for the LMO electrodes after CP test in 0.5 M KH_2PO_4 electrolyte.

References

[1] M.F. Sunding, K. Hadidi, S. Diplas, O.M. Lovvik, T.E. Norby, A.E. Gunnaes, XPS characterisation of in situ treated lanthanum oxide and hydroxide using tailored charge referencing and peak fitting procedures, J. Electron. Spectrosc. Relat. Phenom. 184(7) (2011) 399-409.

[2] N.A. Liedienov, Z. Wei, V.M. Kalita, A.V. Pashchenko, Q. Li, I.V. Fesych, V.A. Turchenko, C. Hou, X. Wei, B. Liu, A.T. Kozakov, G.G. Levchenko, Spin-dependent magnetism and superparamagnetic contribution to the magnetocaloric effect of non-stoichiometric manganite nanoparticles, Appl. Mater. Today, 26 (2022) 101340.